Long-Term Effects of External Sulfate Attack on Low-Carbon Cementitious Materials at Early Age

François El Inaty, Bugra Aydin, Maryam Houhou, Mario Marchetti, Marc Quiertant, Othman Omikrine Metalssi

applied sciences

MDPI

Article

Long-Term Effects of External Sulfate Attack on Low-Carbon Cementitious Materials at Early Age

François El Inaty [1,2], Bugra Aydin [1], Maryam Houhou [1,3], Mario Marchetti [1], Marc Quiertant [2,4] and Othman Omikrine Metalssi [1,*]

[1] Unité Mixte de Recherche-Matériaux pour une Construction Durable (UMR MCD), Université Gustave Eiffel, Cerema, F-77454 Marne-la-Vallée, France; francois.el-inaty@univ-eiffel.fr (F.E.I.); bugraadn@gmail.com (B.A.); mhouhou@cesi.fr (M.H.); mario.marchetti@univ-eiffel.fr (M.M.)
[2] Institut de Recherche de l'ESTP, F-94230 Cachan, France; mquiertant@estp.fr
[3] Laboratoire d'Innovation Numérique pour les Entreprises et les Apprentissages au Service de la Compétitivité des Territoires (LINEACT) Cesi EA, 7527 Saint-Nazaire, France
[4] Expérimentation et Modélisation pour le Génie Civil et Urbain (EMGCU), Université Gustave Eiffel, F-77454 Marne-la-Vallée, France
* Correspondence: othman.omikrine-metalssi@univ-eiffel.fr

Abstract: Placed in a sulfate-rich environment, concrete reacts with sulfate ions, influencing the long-term durability of reinforced concrete (RC) structures. This external sulfate attack (ESA) degrades the cement paste through complex and coupled physicochemical mechanisms that can lead to severe mechanical damage. In common practice, RC structures are generally exposed to sulfate at an early age. This early exposition can affect ESA mechanisms that are generally studied on pre-cured specimens. Moreover, current efforts for sustainable concrete construction focus on replacing clinker with supplementary cementitious materials, requiring a 90-day curing period, which contradicts real-life scenarios. Considering all these factors, the objective of this study is to explore ESA effects at an early age on cement-blended paste samples using various low-carbon formulations. The characterization techniques used demonstrated that the reference mix (100% CEM I) exhibits the weakest resistance to sulfate, leading to complete deterioration after 90 weeks of exposure. This is evident through the highest mass gain, expansion, cracking, formation of ettringite and gypsum, and sulfate consumption from the attacking solution. Conversely, the ternary mix, consisting of CEM I, slag, and metakaolin, demonstrates the highest resistance throughout the entire 120 weeks of exposure. All the blended pastes performed well in the sulfate environment despite being exposed at an early age. It can be recommended to substitute clinker with a limited quantity of metakaolin, along with blast furnace slag, as it is the most effective substitute for clinker, outperforming other combinations.

Keywords: external sulfate attack; early age; supplementary cementitious materials; physicochemical behavior; long term durability; low carbon cement

Citation: El Inaty, F.; Aydin, B.; Houhou, M.; Marchetti, M.; Quiertant, M.; Omikrine Metalssi, O. Long-Term Effects of External Sulfate Attack on Low-Carbon Cementitious Materials at Early Age. *Appl. Sci.* **2024**, *14*, 2831. https://doi.org/10.3390/app14072831

Academic Editors: Mouhamadou Amar and Nor Edine Abriak

Received: 13 February 2024
Revised: 14 March 2024
Accepted: 26 March 2024
Published: 27 March 2024

1. Introduction

In general, two types of sulfate attacks are distinguished. The first is known as internal sulfate attack (ISA, or ISR for internal sulfate reaction, or DEF for delayed ettringite formation), where sulfate originates from raw materials [1,2]. The second is external sulfate attack (ESA), and the source of sulfate, in this case, is the surrounding environment (groundwater, soil, seawater, etc.) [3,4]. When it comes to external sources, sulfate, a pervasive agent contributing to the deterioration of concrete structures, is inevitable due to its presence in various external sources where constructing RC structures is a necessity. Upon contact with RC structures, sulfate ions penetrate the cementitious matrix through the porous network, initiating chemical reactions with hydrated cementitious materials to produce ettringite and/or gypsum [5–9]. This process induces internal stresses, leading to expansion and cracking in the structure. Consequently, the structural integrity weakens, permeability increases, and a feedback loop ensues, facilitating further migration of sulfate ions. This phenomenon involves complex interactions among physical, chemical, and mechanical factors [10–14]. Despite ESA having historical roots dating back to 1818 [15], it remains a complex issue, influenced by many factors, such as cation type (calcium, sodium, or magnesium sulfate), concentration, pH of the surrounding environment, the type of cement used, and many other [16]. A study by Wu et al. [17] compared the degradation effects of blended cement under sodium sulfate and magnesium sulfate attack. Their findings revealed distinct mechanisms of attack, with magnesium sulfate causing significantly more damage compared to sodium sulfate.

Over the years, considerable efforts have been invested in developing methods for testing ESA resistance of all types of binder and concrete. However, each method comes with its strengths and limits, and many are criticized for their dissimilarity with respect to real-world field exposure conditions. Notably, various testing standards, such as ASTM C 1012, the Asian method, the Swiss method, and CSA A 3004-C8, employ high concentrations of sodium sulfate (greater than 30 g/L) [18] to generate an infinite source of sulfate and accelerate the test. A study conducted by Biczok [19] revealed that the preferential formation of ettringite occurs when a low concentration of sulfate is selected, while higher sulfate concentrations lead to an increased production of gypsum. These elevated concentrations, coupled with other testing conditions like extreme temperatures and harsh dry and wet cycles, are intended to accelerate the attack for concrete durability testing against sulfate. However, it is crucial to acknowledge that such conditions may alter the characteristics of the ESA, raising questions about the representativeness of these methods.

In addition, if not prefabricated, on-site cast concrete is directly exposed to the surrounding environment from an early age [20,21]. A recent investigation compared the resistance of prefabricated and cast-in-site concrete against ESA, revealing that prefabricated concrete demonstrates greater resistance to ESA [22]. Curing is recognized for enhancing the properties of structural concrete, including microstructure, mechanical strength, and durability, by promoting the hydration of cementitious materials, reducing creep and shrinkage, and providing protection against environmental aggressions [23]. However, real practices consist of exposing concrete to sulfate ions in certain environments at an early age. Most studies and standards focus on cured samples, typically after 28 or 90 days of curing before attacking the samples, leaving unanswered questions about the impact of ESA on RC structures during their early stages. A recent study [20] investigated the degradation mechanisms induced by ESA on both cured and uncured cement pastes. Surprisingly, pre-cured cement pastes exhibited rapid degradation, although sulfate ion ingress did not show significant differences when comparing pre-cured samples to the uncured ones. In contrast, Li et al. [24] conducted a study suggesting a minimum initial curing period of 14 days for cement-based materials exposed to sulfate. Their findings indicated that a longer initial curing period correlated with improved resistance to sulfate in the cement-based material.

Speaking of common practices while moving to the current trend to resolve environmental issues, one of the most effective and widely employed strategies today to jointly mitigate the substantial CO_2 emissions from the cement industry and to improve cementitious materials' durability is the partial substitution of clinker with supplementary cementitious materials (SCM) [25]. Due to their pozzolanic effects, these materials not only facilitate the formation of additional C-S-H and reduce the porosity size but also serve as a source of alumina, promoting the development of aluminum-containing phases [26]. The changes in cementitious materials composition significantly influence the mechanisms of ESA. In this context, research indicates that the incorporation of SCM enhances the durability of specimens under sulfate attack by reducing the C_3A content [27]. Additionally, numerous studies have demonstrated that the utilization of slag, metakaolin, silica fume, and fly ash improves durability when it comes to ESA [28–33]. In a recent investigation conducted by Miah et al. [34], specimens incorporating fly ash and slag exhibited enhanced mechanical properties after 90 days. Interestingly, these specimens demonstrated similar properties at

28 days compared to those made with ordinary Portland cement (OPC). Furthermore, these findings corresponded with observations of porosity and capillary water absorption. This suggests that the incorporation of SCM necessitates a 90-day curing period to exhibit their benefits. However, this leaves a gap regarding the mechanisms of ESA on materials cured in sulfate (exposed to sulfate at an early age) since previous studies focus on pre-cured samples when it comes to ESA.

Considering all the factors mentioned above, there is a gap in understanding the impact of ESA on samples exposed to sulfate ions at an early age over an extended period, utilizing an adjusted concentration of sulfate. Additionally, there is a need to investigate how ESA affects the resistance of low-carbon cementitious matrices, aligning with the developed low-carbon cement types. For this, this study aims to address two main objectives. Firstly, this study seeks to gain a comprehensive understanding of the long-term effects of ESA on cement paste samples exposed to sulfate ions at an early age. The second objective is to evaluate the resistance of SCM, namely fly ash, blast furnace slag, and metakaolin, under such attack conditions using low-carbon formulations. To achieve this, OPC pastes, binary, ternary, and quaternary blended cement pastes were utilized to address the objectives of the study. The samples underwent exposure to a sodium sulfate solution with a concentration of 15 g/L from an early age, for a duration of three years. This concentration was selected to both create an infinite source of sulfate and to shorten the duration of the test as much as possible while using a relatively low concentration of sulfate. Mass loss, expansion, and physicochemical changes were periodically monitored throughout the experiment, supplemented by visual inspections. The characterization techniques included thermogravimetric analysis, Fourier transform infrared spectroscopy, and the water-accessible porosity test. Furthermore, Raman spectroscopy was employed to monitor the sulfate content in the solutions in which cementitious material samples were immersed.

2. Materials and Methods

2.1. Materials and Mixes Design

For this study, six cementitious mixes were formulated, as detailed in Table 1. The selection of these formulations closely adhered to the specifications outlined in standards NF EN 197-1 and NF EN 197-5 [35,36], with a particular emphasis on chemical criteria. A water-to-binder (W/B) ratio of 0.55 was adopted across all mixes. This relatively high ratio was chosen to increase the porosity and, as a consequence, to accelerate the sulfate attack while mitigating potential segregation issues.

Table 1. Cementitious materials blend design.

	CEM I (%)	Fly Ash (%)	Blast Furnace Slag (%)	Metakaolin (%)
P1	100	-	-	-
S1	55	45	-	-
S2	55	-	45	-
T1	55	15	30	-
T2	55	-	35	10
Q1	55	15	20	10

The primary materials employed in these mixes were CEM I 52.5 N CE CP2 NF, manufactured by EQIOM, with clinker phases (calculated using the Bogue formula [37]) including C_3S at 56.5%, C_2S at 15.8%, C_3A at 5.0%, and C_4AF at 11.6%. Additionally, fly ash and blast furnace slag were incorporated, and their chemical compositions, as provided by the manufacturer, are detailed in Table 2, along with the chemical composition of the used CEM I. Furthermore, metakaolin from BASF MetaMax, described by the manufacturer as 100% calcined kaolin, was also included in the formulations. Those supplementary cementitious materials are the most used substitutes for clinker.

Table 2. Chemical composition of the used materials as given by the manufacturers.

Components	CEM I (w%) [1]	Fly Ash (w%) [1]	Blast Furnace Slag (w%) [1]
SiO_2	20.38	70.83	35.71
Al_2O_3	4.30	24.36	10.65
Fe_2O_3	3.80	2.24	0.45
TiO_2	0.24	1.48	0.73
MnO	0.08	0.05	0.23
CaO	62.79	0.06	43.32
MgO	1.25	0.23	3.97
SO_3	3.46	-	3.06
K_2O	0.73	0.64	0.45
Na_2O	0.35	0.1	0.16
P_2O_5	-	0.05	0.02
S^{2-}	Traces	-	-
Cl^-	0.05	-	-
Loss of ignition	2.54	-	-
Free lime	1.39	-	-

[1] Weight percent.

2.2. Mixing, Casting, and Exposure Procedures

The study was carried out on $40 \times 40 \times 160$ mm^3 prismatic specimens. The preparation protocol of specimens closely adheres to the NF EN 196-1 standard [38] and unfolds as follows: initially, water and cementitious materials are mixed at a low speed of 100 rpm for a duration of 60 s. Subsequently, the speed is increased to 300 rpm for an additional 30 s. Following this, the mixture is allowed to sit undisturbed for 90 s, with the edges of the mixer bowl scraped during the initial 20 s of this interval. The subsequent step involves a second round of high-speed (300 rpm) mixing lasting for 60 s. Various adjustments in mixing speed were used to guarantee the homogenization of the cementitious materials. Employing different mixing speeds helps minimize losses and promotes an even dispersion of components, thereby preventing uneven distribution. Such adjustments are crucial for maintaining the properties of the resulting paste. The resulting paste is poured in one layer into the molds without vibration, but rather, is subjected to four external shocks using a hammer. After a curing period of 24 h, demolding occurs, and the specimens are immediately immersed in sodium sulfate solutions with a concentration of 15 g/L (corresponding to approximately 10.14 g/L of sulfate ions). The water-to-solid volume ratio is maintained at 8 to simulate exposure to an almost infinite sulfate source. To ensure uniform exposure, the specimens are positioned on plastic supports in the attacking solution. The entire setup is preserved at a constant temperature of 20 °C and carefully monitored (expansion and mass gain for the samples and Raman spectroscopy to check the variation of sulfate concentration in the attacking solutions, refer to Section 2.3) and characterized throughout the study. The sodium sulfate solution is renewed weekly for the initial three months, bi-weekly for the subsequent six months, and then monthly, thereafter, to ensure exposure conditions equivalent to an infinite sulfate source, especially since the used concentration of sulfate is relatively low.

2.3. Characterizations Methods

In conjunction with the chemical and microstructural analyses detailed below, this study included mass and expansion monitoring, supplemented by visual observations, all performed at two-week intervals (for the mass and expansion variations) throughout the 120-week experimental phase. The expansion measurement assesses the axial expansion of the prismatic sample, with two axial bolts (or pins) fixed at the two extremities of the sample during casting. The measurements are recorded using an extensometer. The timing of the chemical and microstructural analyses (except for Raman spectroscopy) was determined based on the evolution of patterns of mass and expansion. Thermogravimetric analysis

(TGA) and Fourier transform infrared spectroscopy (FTIR) were conducted on powders extracted from the specimens at depths of 1 (surface), 2, 5, and 15 mm after drying them at a controlled temperature of 55 ± 5 °C for a period of 48 h. The extracted dry material was carried out utilizing the Accutom-100 microtome and a FRITSCH Pulverisette 6 planetary ball mill operating at a speed of 350 rpm for a duration of 2 min.

2.3.1. Thermogravimetric Analysis

TGA was employed as a chemical characterization technique, utilizing the NETZSCH STA 449 F1 apparatus (NETZSCH, Selb, Germany). The analysis spanned a temperature range of 25 to 1250 °C, with a heating rate of 10 °C per minute, all conducted under an inert nitrogen atmosphere. The derivative of the thermogravimetric analysis curve (DTG) was obtained to easily identify crucial mass losses occurring during the heating process.

2.3.2. Fourier Transform Infrared Spectroscopy

FTIR was employed as a chemical characterization technique to identify potential formations of ettringite and gypsum while making comparisons with the original chemical compounds present in the specimens. The Thermo Fisher Scientific Nicolet iS50 spectrometer (Waltham, MA, USA) was utilized for FTIR analysis, covering a spectral range between 400 and 4000 cm^{-1}. The tests were conducted using the integrated diamond ATR.

2.3.3. Raman Spectroscopy

Raman spectroscopy serves as a non-destructive chemical characterization method, including for civil engineering materials. In this study, it was employed to track sulfate consumption in the attacking solutions as an indicator of the extent of the ESA on each mix. Analyses were performed every 30 days (with every solution's renewal). The utilized equipment was an iRaman from BWTek (Newark, DE, USA), operating with a 50 mW laser at 532 nm, featuring a spectral range of 150–4000 cm^{-1} and a spectral resolution of 4 cm^{-1}, using a BAC101 immersion probe.

2.3.4. Water Porosity

The water porosity test, a microstructural assessment, was conducted in accordance with NF P18-459 standard [39]. Samples measuring $40 \times 40 \times 40$ mm^3 were cut from the original $40 \times 40 \times 160$ mm^3 prisms. These samples underwent oven drying at 105 °C until achieving a stable mass. Subsequently, they were placed into a desiccator and subjected to a vacuum for 4 h. The next step involved immersing the samples in water under a pressure of 25 mbar for 48 h. Throughout this process, mass measurements were recorded at various stages: the first being the mass of the dried samples, the second for the mass of the water-saturated samples, and the third capturing the mass of the water-saturated samples submerged in water. A precision scale, with an accuracy of 0.01 g, was employed, and the tests were also conducted at room temperature (20 °C ± 1 °C).

3. Results

3.1. Expansion

Expansion measurements were periodically recorded over the full 120-week duration of the study. The expansion evolution of the samples over time is presented in Figure 1. The provided values are derived from three measurements conducted on distinct samples.

Figure 1 clearly shows that the expansion behavior of the reference mix P1 differs significantly from that of the binary, ternary, and quaternary blended pastes, particularly after week 54. The expansion rate of P1 can be divided into five phases. These phases closely resemble those documented in the current literature [6]. In the initial phase, spanning the first 4 weeks, there is a substantial expansion, reaching 0.08%. The second phase involves a slower but continuous expansion, reaching 0.12% after 54 weeks of sulfate exposure. The third phase extends from week 54 to 72, characterized by a rapid and pronounced expansion, peaking at 0.29%. The fourth phase, between weeks 72 and 84, is characterized by stability, remaining around 0.3%. The fifth phase occurs after that period, reaching an expansion of 0.95% by week 90, at which point the samples were completely degraded. The behavior of the blended pastes (S1, S2, T1, T2, and Q1) exhibited two major phases globally (with three fluctuations in general). The first phase, similar to the reference mix P1, occurred during the initial 4 weeks, where the expansion was around 0.05%. Subsequently, insignificant changes were recorded until week 120, when the expansion reached 0.145%. Throughout this phase, three minor fluctuations were observed. The first fluctuation extended from week 4 to week 54, during which the expansion increased slowly. The second phase persisted until week 70, remaining almost stable before experiencing a subsequent increase at a higher rate.

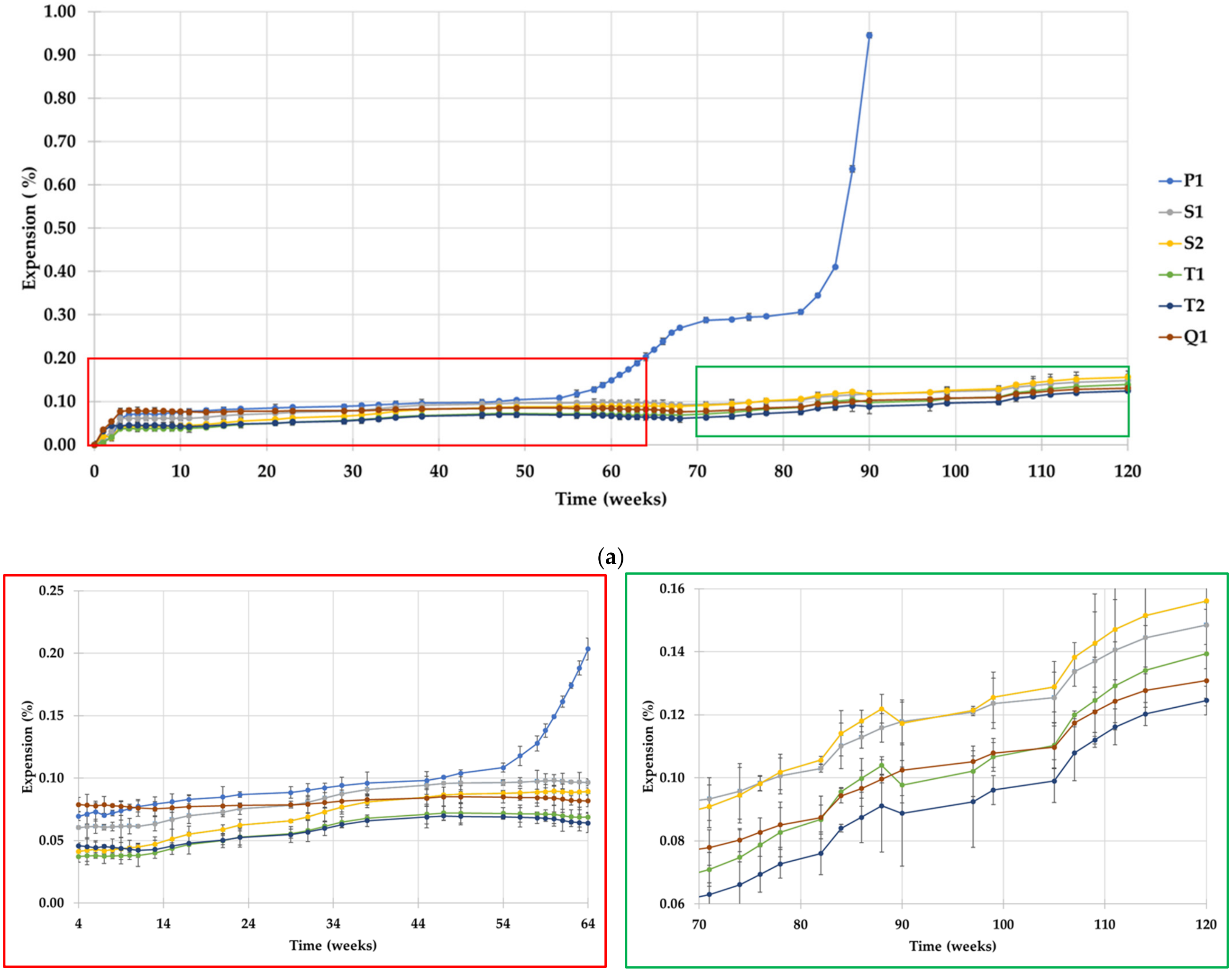

(**a**)

(**b**) (**c**)

Figure 1. Longitudinal expansion of the six mixes over time during the ESA: (**a**) Results of the measurements over the total duration of the test; (**b**) Zoom of the results over the first 64 weeks; (**c**) Zoom of the results from week 70 to week 120.

Based on the description of the expansion rates provided earlier, a common pattern emerged between the expansion rates of the reference mix and the blended ones. After each increase in the expansion rates, a period of stability is observed, followed by a subsequent increase. This pattern is likely attributed to the formation of ettringite and/or gypsum in the pores, leading to internal stresses and causing cracking [20,40] (resulting in an increase in expansion). Subsequently, these products begin to fill the formed cracks (resulting in the stability of the expansion) until they recreate internal stresses and induce new cracks (leading to an increase in expansion). This phenomenon gains further confirmation when examining the continuous mass gain of the samples (refer to Section 3.2).

When comparing the mixes among themselves, the reference mix exhibits the least favorable behavior in terms of expansion and overall durability against ESA. While the other mixes maintained satisfactory expansion rates for 120 weeks, the reference mix P1 expanded by 0.95% after only 90 weeks and deteriorated thereafter. Regarding the blended pastes, as depicted in Figure 1 and considering the scale and low expansion rates, it is evident that they exhibit almost similar behavior. Upon closer examination, mix T2 (composed of CEM I, blast furnace slag, and metakaolin) stood out with the lowest expansion rates. These findings could suggest that the combination of blast furnace slag and a low quantity of metakaolin contributes to the enhanced durability of the overall mix (as previously shown in a study considering 10 to 15% of metakaolin replacement of cement [29]). This is particularly evident when comparing the behavior of other blended mixes that lack this specific combination of slag and metakaolin.

3.2. Mass Changes and Visual Inspection

The mass of all samples was regularly measured over 120 weeks. The mass evolution over time is illustrated in Figure 2 for the six different mixes. Each reported value is the average of three measurements from three different samples.

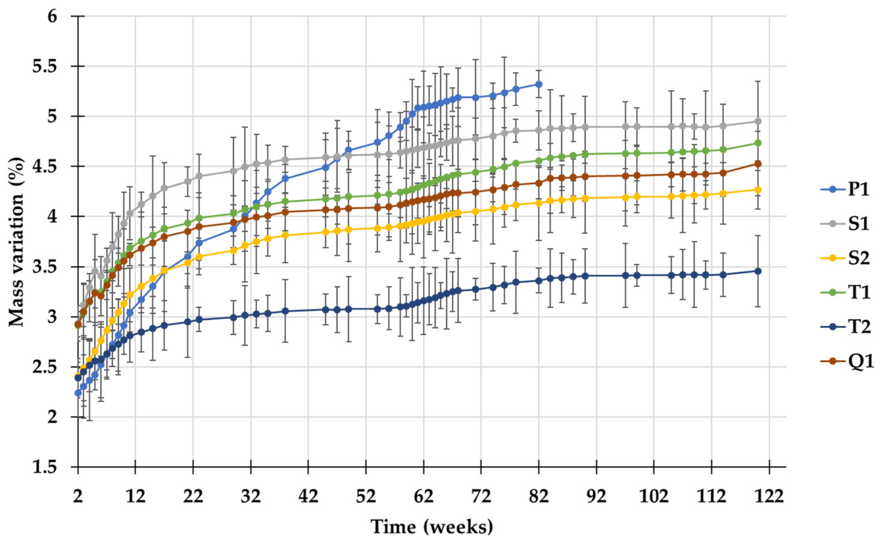

Figure 2. Mass of the six mixes during the ESA over time.

Figure 2 indicates that all samples experienced a mass increase throughout the entire attack period. This phenomenon is expected, as ESA leads to a mass gain, as shown by previous studies [41–43]. However, the rate of mass gain varied among the mixes. Binary (S1 and S2), ternary (T1 and T2), and quaternary (Q1) blended pastes exhibited similar rates of mass gain, distinct from the reference mix (P1) composed of 100% clinker. Blended pastes demonstrated a significant mass gain in the initial 35 weeks, stabilizing thereafter with a slight increase up to week 120. In contrast, the mass gain kinetics of the reference mix (P1) were different from the other formulations, showing a rather regular mass gain during the 62 weeks and a beginning of stabilization afterward. Mass measurements for P1 were terminated at week 82 due to the samples' full deterioration caused by ESA.

The initial 12 weeks witnessed substantial mass gain for all mixes, attributable to various factors. The samples, immersed in sulfate at an early age (24 h after casting), experienced both the hydration of cementitious pastes, leading to the formation of hydrated products, and water absorption [42,44]. Additionally, this gain can be associated with the chemical reaction between hydrated cementitious materials and sulfate, resulting in the formation of ettringite and gypsum within micro-pores and cracks, contributing to the observed mass gain [16,40,45]. Following this period, marking the completion of the hydration of cementitious materials (lasting 90 days, notably longer for blended pastes compared to 28 days for P1, as discussed by Miah et al. [34]), the blended mixes continued to experience mass gain but at reduced rates before almost stabilizing (having however minor gain), as discussed earlier. At this stage, with hydration nearly complete and the samples saturated, the observed mass gain could be attributed to the formation of gypsum and ettringite resulting from the chemical reaction between the hydrated products and sulfate. It is important to note that 90 days after the fabrication (upon completion of hydration), a significant reduction in porosity and capillary water absorption in the blended pastes is observed, according to previous studies [34]. This decrease in porosity contributes to stabilizing the mass gain. The above-explained results highlight that the reference mix (P1) exhibited the least favorable behavior in terms of mass gain and overall durability, as evidenced by its degradation after 90 weeks of exposure. In contrast, the other mixes, which incorporate SCM to partially substitute the clinker, demonstrated a more robust performance, maintaining their structural integrity even after 120 weeks of sulfate exposure.

Upon comparing the mass gains of the blended pastes, it becomes evident that the ternary mix (T2), composed of CEM I, blast furnace slag, and metakaolin, exhibited the lowest mass gain from the initiation of the sulfate attack. In contrast, the mix containing CEM I and fly ash (S1) displayed the highest mass gain among the blended mixes. This, coupled with the mass gain rates of the other blended mixes, could imply that the inclusion of blast furnace slag and metakaolin, within specified replacement percentages, enhanced the overall performance of the mixes.

In terms of visual inspection, the reference mix P1 exhibited the highest visual aging rate, as depicted in Figure 3. After 60 weeks of exposure, P1 underwent a significant color change compared to the minor changes observed in the other mixes, which exhibited similar behavior in terms of color alteration and crack development. Furthermore, after 95 weeks of exposure, mix P1 experienced complete degradation, while the rest of the mixes only displayed some cracking on the edges of the specimens. Additionally, even after 120 weeks, the blended mixes did not exhibit more than insignificant cracking, as illustrated with the mix Q1.

Figure 3. Visual inspection of P1 (reference mix) and Q1 after 4, 60, 95, and 120 weeks of exposure (the red circles highlight areas where cracks are observed in mix Q1).

In general, the expansion rates and the steps of increase aligned with the mass gain rates and visual observations. During the initial weeks, as the specimens underwent the curing process in a sulfate-enriched solution (initiated 24 h after casting), there was ongoing hydration, water absorption, and the formation of ettringite and gypsum due to sulfate (contributing to mass gain, internal stresses leading to expansion, and observable visual changes) [42]. Following this initial period (4 weeks for the reference mix P1 and approximately 12 weeks for the blended pastes), subsequent changes are primarily attributed to the reaction between sulfate and the hydrated products, leading the consequences of the ESA [46,47].

Based on those results, including expansion, mass variation, and visual observations, analyses such as TGA, FTIR, and water porosity were conducted at three key time points: 24 h after casting (Ti0), 8 weeks into the initiation of ESA (Ti1), and at 80 weeks (Ti2).

3.3. Thermogravimetric Analysis

TGA was conducted on the six mixes at two different time points: 8 (Ti1) and 80 (Ti2) weeks of immersion in the sulfate solution. The analysis included measurements on materials extracted at various depths within the $40 \times 40 \times 160$ cm^3 specimens, specifically at 1 (surface), 2, 5, and 15 mm.

According to some previous research [48,49], when examining the DTG curve, the initial peak, observed between 30 °C and 200 °C, signifies the decomposition of ettringite, C-S-H, and free water. Furthermore, the presence of monosulfoaluminates (AFm) was indicated by a peak at around 190 °C. The dihydroxylation process of portlandite ($Ca(OH)_2$) manifests as the third peak between 450 °C and 550 °C, while the decarbonation of calcite ($CaCO_3$) was responsible for the peak observed between 650 °C and 820 °C.

When investigating ESA, a careful analysis of portlandite consumption is imperative, as it provides valuable insights into the progression of this attack [16]. Additionally, AFm serves as a source of alumina during the sulfate attack, contributing to the formation of ettringite [50]. The results related to portlandite content are presented in Figure 4.

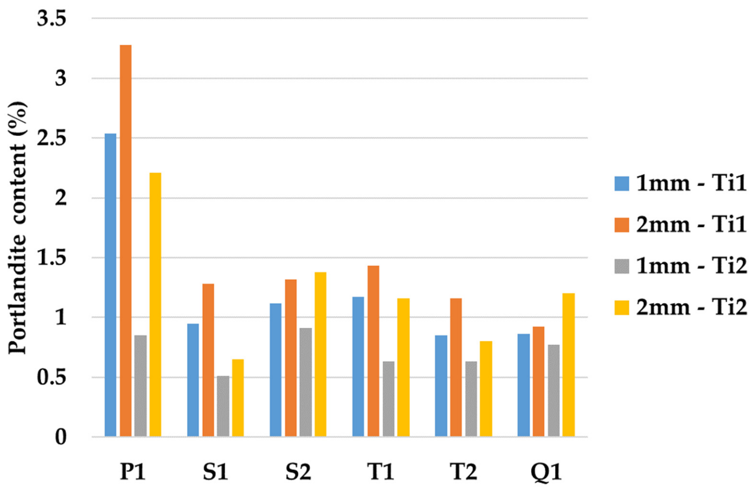

Figure 4. Portlandite content (%) of the six mix samples at 1 mm and 2 mm depths after being submerged in sulfate for 8 weeks (Ti1) and 80 weeks (Ti2).

Upon a general examination of portlandite content, carried out using the TGA test, it can be shown that the progression of the attack at 80 weeks overtakes that observed at 8 weeks, aligning with expectations. A more detailed analysis comparing depths at 1 mm and 2 mm reveals a heightened aggression of the attack at the initial 1 mm, in direct contact with sulfate. This is notably reflected in the portlandite content at these respective depths. Furthermore, the reference mix P1 exhibits a significantly higher overall portlandite content compared to the blended mixes. This is attributed to the absence of the pozzolanic effect of SCM, which typically favors the formation of C-S-H [34,51].

From the data presented in Figure 4, it becomes evident that the reference mix P1 exhibits weaker durability against sulfate attack. This conclusion is drawn from the higher portlandite loss observed in this mix, not only at different depths (1 and 2 mm) but also at different time points (Ti1 and Ti2). In the initial 8-week step, the portlandite content increased from 2.5% to 3.3% at depths of 1 and 2 mm, respectively. Subsequently, at Ti2, the portlandite content further increased from 0.85% at 1 mm to 2.2% at 2 mm. This consistent increase in portlandite content indicates a more pronounced degradation of the reference mix under sulfate attack conditions. However, when examining the blended mixes, their behavior in terms of portlandite loss appears to be quite similar. Considering the ternary mix T2, characterized by the best resistance based on the previously discussed results, its portlandite content, for instance, increased marginally from 0.63% at 1 mm depth to 0.8% at 2 mm depth at time Ti2, representing a minimal loss of 0.17%. This indicates a more robust performance of the blended mixes, particularly exemplified by mix T2, against sulfate attack conditions compared to the reference mix.

Analyzing the first peak of the DTG curve (refer to Figure 5), it is evident that the content of ettringite, C-S-H, and free water at all depths of the reference mix P1 is greater than in other mixes. Considering that all mixes underwent the same conditions and drying procedures and acknowledging that the C-S-H content is higher in the blended pastes [51], it can be concluded that the ettringite content in the reference mix is elevated, extending even to a depth of 15 mm. This indicates not only the poor resistance of P1 when it comes to ESA but also suggests that the attack has reached the core of the reference mix. In contrast, the attack remains superficial in the blended mixes even after 120 weeks. This conclusion is further supported by examining the AFm content (peak around 190 °C on the DTG curve), which does not exist in the reference mix, even at 15 mm, but is present in the other mixes at 5 and 15 mm depths. To validate these findings, an FTIR test is conducted and discussed in the following section.

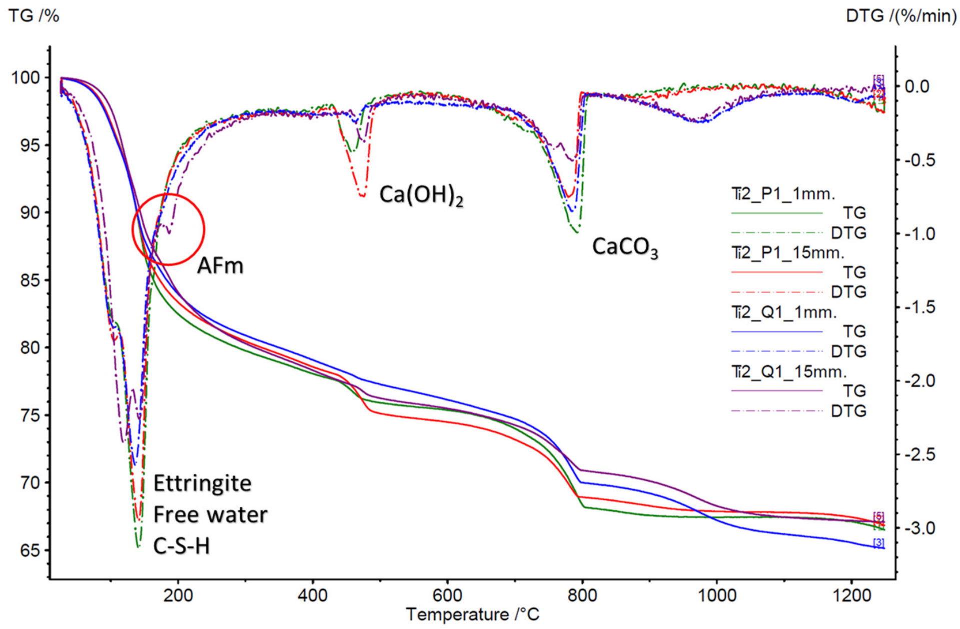

Figure 5. TG and DTG curves of the reference mix (P1) and of Q1 at 1 mm and 15 mm depths after 80 weeks of immersion in sulfate solution.

3.4. Fourier Transform Infrared Spectroscopy

FTIR analysis was conducted on the whole six mixes after 8 (Ti1) and 80 (Ti2) weeks of immersion in the sulfate solution at 1, 2, 5, and 15 mm depths.

In accordance with findings from previous studies [52–54], various chemical compounds and phases within the cementitious samples can be identified through FTIR. Portlandite, characterized by O-H stretching, is identified with a peak at 3642 cm^{-1}. The compounds AFm, ettringite, and gypsum, exhibiting S-O vibration, manifest by the peak of 1102 cm^{-1}. The presence of water is indicated by a broad band at the peak of 3373 cm^{-1} attributed to the stretch mode of the O-H bond. Ettringite, distinguished by S-O vibration, can be detected at the peak of 619 cm^{-1}, while gypsum shows up at the band of 1685 cm^{-1}. These distinctive peaks and bands provide valuable insights into the chemical composition and phases present in the cementitious samples, contributing to a comprehensive understanding of their behavior under ESA.

The analysis of the FTIR spectra presented in Figure 6a, which depicts the chemical composition of the reference mix P1 at 1, 2, and 5 mm after 80 weeks of exposure to sulfate, reveals a significant attack at 1 mm and a diminishing impact with increasing depth. This observation is distinguished by examining the intensity of peaks corresponding to gypsum (at 1685 cm^{-1}), ettringite, gypsum, and AFm (AFm's presence is questionable based on TGA results discussed in Section 3.3) at 1102 cm^{-1}, as well as ettringite at 619 cm^{-1}. Figure 6c, representing the same mix at 1 mm depth but comparing 8 weeks of exposure to 80 weeks, demonstrates that the attack has progressed and become more pronounced after 80 weeks of exposure. To assess the impact of SCM on enhancing durability against ESA, Figure 6d illustrates P1 and the quaternary mix Q1 at 1 mm depth after 80 weeks of exposure, highlighting a significant difference. Notably, the formation of ettringite and gypsum in the reference mix is substantial, showcasing the effectiveness of substituting clinker with SCM at specific percentages. This aligns with the overarching findings of the study. Further insights can be gained by examining Figure 6b, which compares the degree of formation of expansive products at different depths of the ternary mix T1 and the mix P1 shown in Figure 6a.

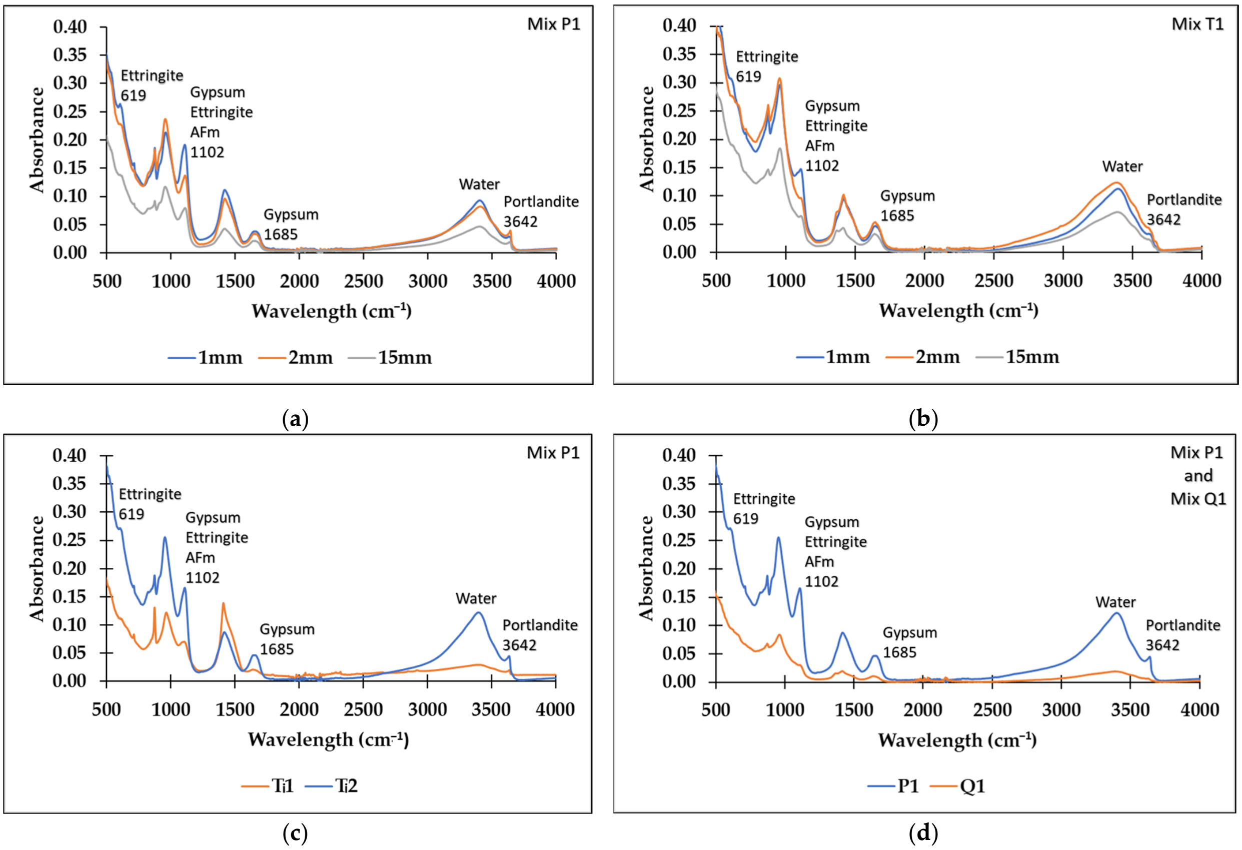

Figure 6. FTIR spectra, showcasing (**a**) the reference mix (P1) and (**b**) mix T1 at various depths after 80 weeks of exposure to sulfate. Additionally, it includes (**c**) mix P1 at 1 mm depth after 8 and 80 weeks of sulfate exposure, and (**d**) mix P1 and mix Q1 at 1 mm depth after 80 weeks of contact with sulfate.

3.5. Raman Spectroscopy

Raman spectroscopy was employed to analyze the solutions before each renewal (every 30 days), allowing for the monitoring of sulfate consumption.

According to previous studies [55,56], the presence of sulfate is identified by a peak found between 980 and 1160 cm^{-1}. Moreover, water is identified by the large peak found around 3400 cm^{-1} due to the vibration stretching mode of the O-H bond.

The results of the Raman spectroscopy, illustrated in Figure 7 and conducted at each renewal of the solutions, reveal the persistent presence of sulfate, indicated by its peak, which is never fully consumed by the samples. Interestingly, the intensity of the peak varies among the solutions and depends on the mix used to prepare the samples in contact with those solutions. The attacking solution in contact with the reference mix shows the lowest sulfate concentration after 30 days, suggesting that the reference mix consumes more available sulfate than the other mixes, up to the point that the sulfate consumption of the solution, considered as an infinite source of sulfate, become detectable. Moreover, the solution in contact with the ternary mix T2 exhibits the highest sulfate concentration after exposure, indicating that this mix has the highest resistance to sulfate. This aligns with the findings of the previous characterization tests discussed earlier. It also implies that the detection of ESA can be conducted by spectral monitoring of the sulfate solution without having to go through as many sample characterizations.

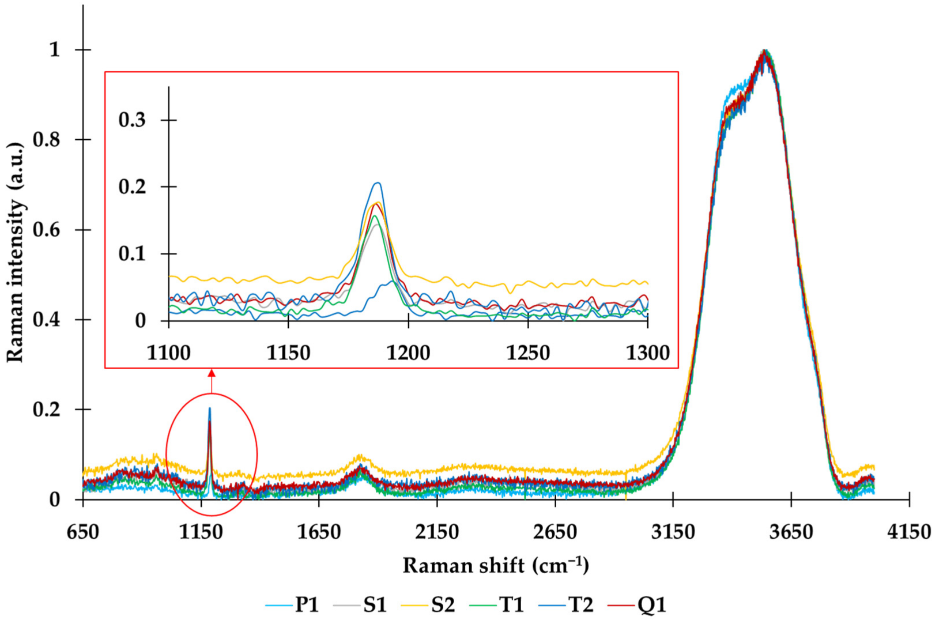

Figure 7. Raman specters of the sulfate solutions that are in contact with all the mixes after 80 weeks.

3.6. Water Porosity

A water porosity test was performed on all the mixes after 8 (Ti1) and 80 (Ti2) weeks of immersion in the sulfate solution in addition to 24 h after casting (Ti0).

As illustrated in Figure 8, the initial porosity of the samples was notably high, approximately around 51% at time Ti0, consistent with select a W/B ratio of 0.55. A previous study conducted by Nehdi et al. [57] demonstrated that increasing the W/B ratio leads to an increase in total porosity. The porosity then decreased by approximately 8% when cured in water (refer to Ti2 Ref) due to the ongoing hydration process. The significant initial porosity can be attributed to the fact that the samples were poured into the molds without vibration, as mentioned in Section 2.2. Additionally, it is evident that the porosity varies among the samples, and its evolution differs. This variability is attributed to differences in workability resulting from the substitution of clinker in the various mixes [58].

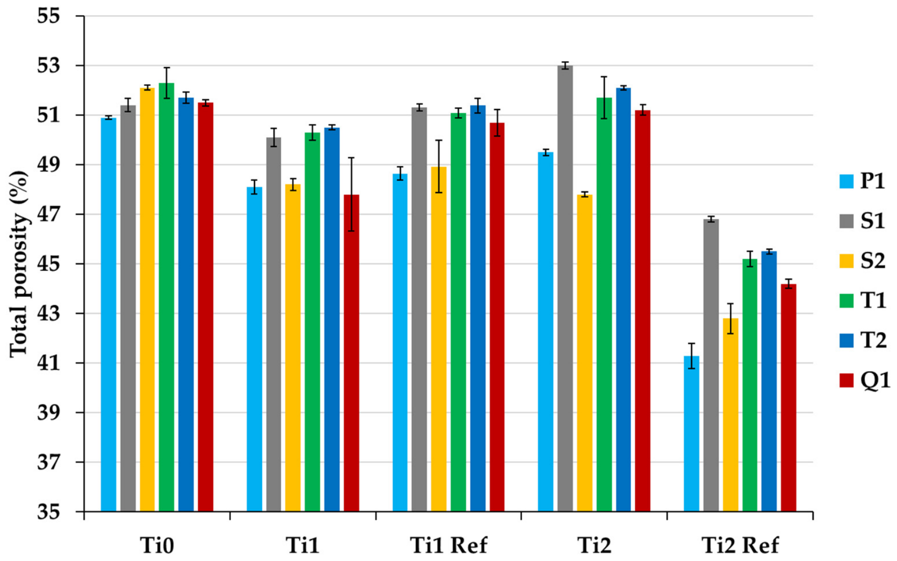

Figure 8. Total water porosity (%) of all the mixes 24 h after fabrication (Ti0), 8 (Ti1), and 80 (Ti2) weeks of being in contact with sulfate and in water.

Comparing water porosity results at 8 weeks between mixes exposed to sulfate (Ti1) and mixes cured in water (Ti1 Ref) reveals interesting trends. Notably, the reference mix, P1, showed slightly higher porosity in the water-cured environment (~49%) compared to its sulfate-exposed counterpart (~48%). A similar pattern was observed in other mixes, including S1, S2, T1, T2, and Q1, where slightly higher porosity values were seen underwater curing than with sulfate exposure. This is attributed to the formation of ettringite and gypsum due to sulfate exposure. The most significant increase in porosity occurred in S1, where the sulfate-exposed mix (~50%) surpassed the water-cured mix (~51%) by 1.2 percentage points. This aligns with the expansion rates and mass gain of mix S1, which exhibited the highest values among all mixes in the early stages of the attack. Similar findings have been documented by other studies, which have compared the porosity of mixes containing 100% CEMI with those incorporating supplementary cementitious materials [57].

However, examining water porosity results after 80 weeks of sulfate exposure (Ti2) and comparing them with mixes cured in water for the same duration (Ti2 Ref) reveals different trends when compared to Ti1 and Ti1 Ref. The reference mix (P1) demonstrated higher porosity in the sulfate-exposed environment (49.5%) compared to its water-exposed counterpart (~41%). This unexpected trend extended to other mixes, including S1, S2, T1, T2, and Q1, where sulfate-exposed mixes exhibited higher porosity values than their water-exposed counterparts. The most important increase in porosity was observed in P1, with the sulfate-exposed mix exceeding the water-cured mix by 8.2 percentage points. This is likely due to the formation of cracks due to ESA. These results are in accordance with all the previous findings of this study, including extensive mass and expansion gain, high formation of ettringite and gypsum, as well as visual deterioration of the reference mix. Moreover, the blended mixes exhibited similar behavior in the long-term exposure to sulfate, as previously demonstrated, with good values regarding porosity at this stage, with mix S2 leading. However, the difference between the blended mixes during the water porosity test is minor.

The water porosity results are valuable for comparing two time-points. However, this parameter cannot be considered a major durability indicator concerning ESA. This is because there can be significant fluctuations in the porosity. These fluctuations may be attributed to various phenomena, including the pore-filling effect by the formation of ettringite and/or gypsum, cracks opening due to the crystallization pressure of the expensive products coming from ESA, subsequent sealing of these cracks, the creation of new cracks, and so forth.

3.7. Results Overview Illustration

From the findings of this study, a visual representation was generated to describe the obtained results. The illustration provides a concise overview of the key outcomes and insights derived from the comprehensive analyses conducted in this study. It is presented in Figure 9.

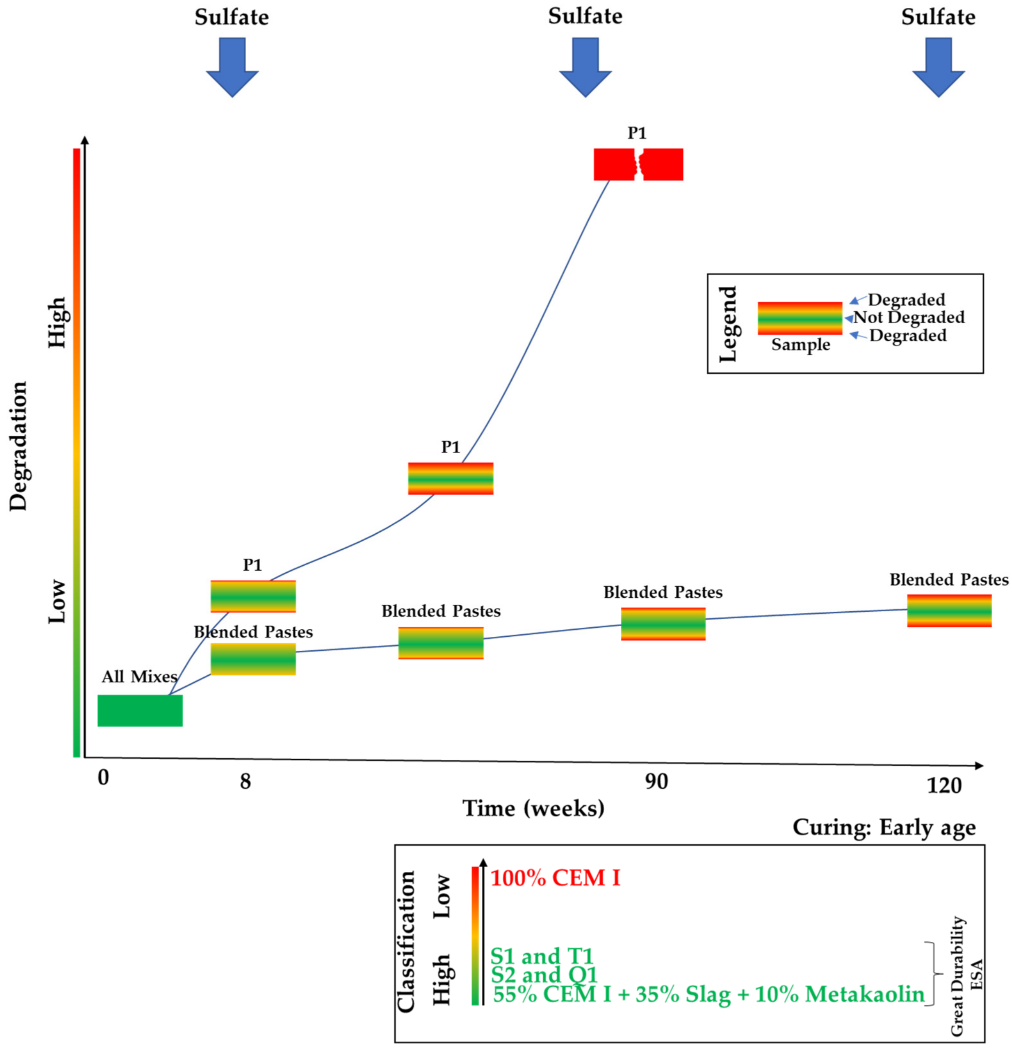

Figure 9. Illustrative overview of research results.

4. Conclusions

In this investigation, OPC pastes, as well as binary, ternary, and quaternary blended cement pastes, underwent long-term exposure to 15 g/L of sodium sulfate at an early age. Following comprehensive characterizations and continuous monitoring of the attacked samples, the study resulted in the following conclusions:

- CEM I exhibits the lowest resistance to ESA when compared to blended mixes. It shows the highest mass gain, expansion, formation of ettringite and gypsum, sulfate consumption from the solution, and microstructure alteration. Additionally, during the course of this experiment, it deteriorated only after 90 weeks, whereas the blended cements maintained their structural integrity even after 120 weeks;
- blended specimens demonstrated good durability, retaining structural integrity after 120 weeks of sulfate exposure from an early age;
- incorporating a low quantity (10%) of metakaolin along with blast furnace slag emerged as the most effective substitute for clinker, outperforming other combinations based on the observed behavior of various blended mixes in sulfate exposure;

- non-invasive Raman spectroscopy emerged as a reliable method for monitoring the ESA effect by quantifying the sulfate ions left in the attacking solutions.

Further investigations at the mortar and/or concrete scale would provide additional insights into the physical transport properties, in addition to the chemical aspects of ESA. This is particularly relevant as the current study focuses on cement paste materials that are highly porous. Moreover, further investigations are needed to explore the effects of adding metakaolin to slag as a substitute for clinker, aiming to develop highly resistant materials against ESA.

Author Contributions: Validation, conceptualization, methodology, writing—review, editing, and supervision O.O.M., M.M. and M.Q.; conceptualization, methodology, writing—original draft preparation, investigation, formal analysis, and editing, F.E.I.; validation, investigation, writing—review, and formal analysis, B.A. and M.H. All authors have read and agreed to the published version of the manuscript.

Funding: This research received no external funding.

Institutional Review Board Statement: Not applicable.

Informed Consent Statement: Not applicable.

Data Availability Statement: Data are contained within the article.

Conflicts of Interest: The authors declare no conflicts of interest.

References

1. Zhao, G.; Li, J.; Shao, W. Effect of mixed chlorides on the degradation and sulfate diffusion of cast-in-situ concrete due to sulfate attack. *Constr. Build. Mater.* **2018**, *181*, 49–58. [CrossRef]
2. Ouyang, C.; Nanni, A.; Chang, W.F. Internal and external sources of sulfate ions in portland cement mortar: Two types of chemical attack. *Cem. Concr. Res.* **1988**, *18*, 699–709. [CrossRef]
3. Geng, J.; Easterbrook, D.; Li, L.; Mo, L. The stability of bound chlorides in cement paste with sulfate attack. *Cem. Concr. Res.* **2015**, *68*, 211–222. [CrossRef]
4. Wongprachum, W.; Sappakittipakorn, M.; Sukontasukkul, P.; Chindaprasirt, P.; Banthia, N. Resistance to sulfate attack and underwater abrasion of fiber reinforced cement mortar. *Constr. Build. Mater.* **2018**, *189*, 686–694. [CrossRef]
5. Skaropoulou, A.; Sotiriadis, K.; Kakali, G.; Tsivilis, S. Use of mineral admixtures to improve the resistance of limestone cement concrete against thaumasite form of sulfate attack. *Cem. Concr. Compos.* **2013**, *37*, 267–275. [CrossRef]
6. Santhanam, M.; Cohen, M.D.; Olek, J. Mechanism of sulfate attack: A fresh look: Part 1: Summary of experimental results. *Cem. Concr. Res.* **2002**, *32*, 915–921. [CrossRef]
7. Yu, X.; Chen, D.; Feng, J.; Zhang, Y.; Liao, Y. Behavior of mortar exposed to different exposure conditions of sulfate attack. *Ocean Eng.* **2018**, *157*, 1–12. [CrossRef]
8. Ikumi, T.; Segura, I.; Cavalaro, S.H.P. Effects of biaxial confinement in mortars exposed to external sulfate attack. *Cem. Concr. Compos.* **2019**, *95*, 111–127. [CrossRef]
9. El Inaty, F.; Marchetti, M.; Quiertant, M.; Omikrine Metalssi, O. Chemical Mechanisms Involved in the Coupled Attack of Sulfate and Chloride Ions on Low-Carbon Cementitious Materials: An In-Depth Study. *Appl. Sci.* **2023**, *13*, 11729. [CrossRef]
10. Neville, A. The confused world of sulfate attack on concrete. *Cem. Concr. Res.* **2004**, *34*, 1275–1296. [CrossRef]
11. Yu, C.; Sun, W.; Scrivener, K. Mechanism of expansion of mortars immersed in sodium sulfate solutions. *Cem. Concr. Res.* **2013**, *43*, 105–111. [CrossRef]
12. Xiong, C.; Jiang, L.; Xu, Y.; Chu, H.; Jin, M.; Zhang, Y. Deterioration of pastes exposed to leaching, external sulfate attack and the dual actions. *Constr. Build. Mater.* **2016**, *116*, 52–62. [CrossRef]
13. Shao, W.; Li, Q.; Zhang, W.; Shi, D.; Li, H. Numerical modeling of chloride diffusion in cement-based materials considering calcium leaching and external sulfate attack. *Constr. Build. Mater.* **2023**, *401*, 132913. [CrossRef]
14. El Inaty, F.; Baz, B.; Aouad, G. Long-term durability assessment of 3D printed concrete. *J. Adhes. Sci. Technol.* **2022**, *37*, 1921–1936. [CrossRef]
15. Al-Amoudi, O.S.B. Sulfate attack and reinforcement corrosion in plain and blended cements exposed to sulfate environments. *Build. Environ.* **1998**, *33*, 53–61. [CrossRef]
16. Jabbour, M. Multi-Scales Study for the External Sulfatic Attack in Reinforced Concrete Structures. Ph.D. Thesis, Université Paris-Est, Paris, France, 2019. Available online: https://tel.archives-ouvertes.fr/tel-02956401 (accessed on 2 November 2023).
17. Wu, M.; Zhang, Y.; Ji, Y.; She, W.; Yang, L.; Liu, G. A comparable study on the deterioration of limestone powder blended cement under sodium sulfate and magnesium sulfate attack at a low temperature. *Constr. Build. Mater.* **2020**, *243*, 118279. [CrossRef]

18. Jabbour, M.; Metalssi, O.O.; Quiertant, M.; Baroghel-Bouny, V. A Critical Review of Existing Test-Methods for External Sulfate Attack. *Materials* **2022**, *15*, 7554. [CrossRef] [PubMed]
19. Imre BICZOK. *Concrete Corrosion and Concrete Protection*; Chemical Publishing Compan: New York, NY, USA, 1967. Available online: https://scholar.google.com/scholar_lookup?title=Concrete+Corrosion+and+Concrete+Protection&author=Biczok,+I.&publication_year=1967 (accessed on 20 November 2023).
20. Metalssi, O.O.; Ragoug, R.; Barberon, F.; d'Espinose de Lacaillerie, J.-B.; Roussel, N.; Divet, L.; Torrenti, J.-M. Effect of an Early-Age Exposure on the Degradation Mechanisms of Cement Paste under External Sulfate Attack. *Materials* **2023**, *16*, 6013. [CrossRef]
21. Li, Z.; Zhou, X.; Ma, H.; Hou, D. *Advanced Concrete Technology*; John Wiley & Sons: Hoboken, NJ, USA, 2022.
22. Zhao, G.; Shi, M.; Guo, M.; Fan, H. Degradation Mechanism of Concrete Subjected to External Sulfate Attack: Comparison of Different Curing Conditions. *Materials* **2020**, *13*, 3179. [CrossRef]
23. Pawar, Y.; Kate, S. Curing of Concrete: A Review. *Int. Res. J. Eng. Technol.* **2020**, *7*, 1820–1824. [CrossRef]
24. Li, X.; Yu, X.; Zhao, Y.; Yu, X.; Li, C.; Chen, D. Effect of initial curing period on the behavior of mortar under sulfate attack. *Constr. Build. Mater.* **2022**, *326*, 126852. [CrossRef]
25. Scrivener, K.; Martirena, F.; Bishnoi, S.; Maity, S. Calcined clay limestone cements (LC3). *Cem. Concr. Res.* **2018**, *114*, 49–56. [CrossRef]
26. Zou, Y.-X.; Zuo, X.-B.; Zhang, H.-L.; Wang, S.-Q. Influence of fly ash and chlorides on the behavior of sulfate attack in blended cement pastes. *Constr. Build. Mater.* **2023**, *394*, 132231. [CrossRef]
27. Elahi, M.M.A.; Shearer, C.R.; Naser Rashid Reza, A.; Saha, A.K.; Khan, M.N.N.; Hossain, M.M.; Sarker, P.K. Improving the sulfate attack resistance of concrete by using supplementary cementitious materials (SCMs): A review. *Constr. Build. Mater.* **2021**, *281*, 122628. [CrossRef]
28. Ramyar, K.; İnan, G. Sodium sulfate attack on plain and blended cements. *Build. Environ.* **2007**, *42*, 1368–1372. [CrossRef]
29. Al-Akhras, N.M. Durability of metakaolin concrete to sulfate attack. *Cem. Concr. Res.* **2006**, *36*, 1727–1734. [CrossRef]
30. Shi, Z.; Ferreiro, S.; Lothenbach, B.; Geiker, M.R.; Kunther, W.; Kaufmann, J.; Herfort, D.; Skibsted, J. Sulfate resistance of calcined clay–Limestone–Portland cements. *Cem. Concr. Res.* **2019**, *116*, 238–251. [CrossRef]
31. Al-Dulaijan, S.U.; Maslehuddin, M.; Al-Zahrani, M.M.; Sharif, A.M.; Shameem, M.; Ibrahim, M. Sulfate resistance of plain and blended cements exposed to varying concentrations of sodium sulfate. *Cem. Concr. Compos.* **2003**, *25*, 429–437. [CrossRef]
32. Lee, S.T.; Moon, H.Y.; Swamy, R.N. Sulfate attack and role of silica fume in resisting strength loss. *Cem. Concr. Compos.* **2005**, *27*, 65–76. [CrossRef]
33. Baghabra Al-Amoudi, O.S. Attack on plain and blended cements exposed to aggressive sulfate environments. *Cem. Concr. Compos.* **2002**, *24*, 305–316. [CrossRef]
34. Miah, M.J.; Huaping, R.; Paul, S.C.; Babafemi, A.J.; Li, Y. Long-term strength and durability performance of eco-friendly concrete with supplementary cementitious materials. *Innov. Infrastruct. Solut.* **2023**, *8*, 255. [CrossRef]
35. *EN 197-1:2011*; European Committee for Standardization. Cement—Part 1: Composition, Specifications and Conformity Criteria for Common Cements. iTeh, Inc.: Newark, DE, USA, 2011.
36. *NF EN 197-5*; European Committee for Standardization. Ciment—Partie 5: Ciment Portland Composé CEM II/C-M et Ciment composé CEM VI. Afnor EDITIONS. AFNOR: Saint-Denis, France, 2021. Available online: https://www.boutique.afnor.org/fr-fr/norme/nf-en-1975/ciment-partie-5-ciment-portland-compose-cem-ii-cm-et-ciment-compose-cem-vi/fa200094/264804 (accessed on 18 October 2023).
37. Bogue, R.H. *The Chemistry of Portland Cement*, 2nd ed.; LWW: Pennvania, PA, USA, 1955; Volume 79, p. 322.
38. *NF 196-1*; Méthodes d'Essais des Ciments. AFNOR: Saint-Denis, France, 2006.
39. *NF P18-459*; Béton-Essai pour Béton Durci—Essai de Porosité et de Masse Volumique. AFNOR: Saint-Denis, France, 2010. Available online: https://www.boutique.afnor.org/fr-fr/norme/nf-p18459/beton-essai-pour-beton-durci-essai-de-porosite-et-de-masse-volumique/fa160729/34961 (accessed on 9 January 2024).
40. Metalssi, O.O.; Touhami, R.R.; Barberon, F.; d'Espinose de Lacaillerie, J.-B.; Roussel, N.; Divet, L.; Torrenti, J.-M. Understanding the degradation mechanisms of cement-based systems in combined chloride-sulfate attack. *Cem. Concr. Res.* **2023**, *164*, 107065. [CrossRef]
41. Jiang, L.; Niu, D. Study of deterioration of concrete exposed to different types of sulfate solutions under drying-wetting cycles. *Constr. Build. Mater.* **2016**, *117*, 88–98. [CrossRef]
42. Zhang, Z.; Jin, X.; Luo, W. Long-term behaviors of concrete under low-concentration sulfate attack subjected to natural variation of environmental climate conditions. *Cem. Concr. Res.* **2019**, *116*, 217–230. [CrossRef]
43. Nosouhian, F.; Mostofinejad, D.; Hasheminejad, H. Concrete Durability Improvement in a Sulfate Environment Using Bacteria. *J. Mater. Civ. Eng.* **2016**, *28*, 04015064. [CrossRef]
44. Haufe, J.; Vollpracht, A. Tensile strength of concrete exposed to sulfate attack. *Cem. Concr. Res.* **2019**, *116*, 81–88. [CrossRef]
45. Santhanam, M.; Cohen, M.D.; Olek, J. Effects of gypsum formation on the performance of cement mortars during external sulfate attack. *Cem. Concr. Res.* **2003**, *33*, 325–332. [CrossRef]
46. Tian, B.; Cohen, M.D. Does gypsum formation during sulfate attack on concrete lead to expansion? *Cem. Concr. Res.* **2000**, *30*, 117–123. [CrossRef]
47. Ma, X.; Çopuroğlu, O.; Schlangen, E.; Han, N.; Xing, F. Expansion and degradation of cement paste in sodium sulfate solutions. *Constr. Build. Mater.* **2018**, *158*, 410–422. [CrossRef]

48. Gao, Y.; Cui, X.; Lu, N.; Hou, S.; He, Z.; Liang, C. Effect of recycled powders on the mechanical properties and durability of fully recycled fiber-reinforced mortar. *J. Build. Eng.* **2022**, *45*, 103574. [CrossRef]
49. Nochaiya, T.; Sekine, Y.; Choopun, S.; Chaipanich, A. Microstructure, characterizations, functionality and compressive strength of cement-based materials using zinc oxide nanoparticles as an additive. *J. Alloys Compd.* **2015**, *630*, 1–10. [CrossRef]
50. Irbe, L.; Beddoe, R.E.; Heinz, D. The role of aluminium in C-A-S-H during sulfate attack on concrete. *Cem. Concr. Res.* **2019**, *116*, 71–80. [CrossRef]
51. Fode, T.A.; Chande Jande, Y.A.; Kivevele, T. Effects of different supplementary cementitious materials on durability and mechanical properties of cement composite–Comprehensive review. *Heliyon* **2023**, *9*, e17924. [CrossRef]
52. Farcas, F.; Touzé, P. La spectrométrie infrarouge à transformée de Fourier (IRTF). *Bull. Lab. Ponts Chaussées* **2001**, *230*, 77–88.
53. Liu, P.; Chen, Y.; Wang, W.; Yu, Z. Effect of physical and chemical sulfate attack on performance degradation of concrete under different conditions. *Chem. Phys. Lett.* **2020**, *745*, 137254. [CrossRef]
54. Yue, Y.; Wang, J.J.; Basheer, P.A.M.; Bai, Y. Raman spectroscopic investigation of Friedel's salt. *Cem. Concr. Compos.* **2018**, *86*, 306–314. [CrossRef]
55. Tang, C.; Ling, T.-C.; Mo, K.H. Raman spectroscopy as a tool to understand the mechanism of concrete durability—A review. *Constr. Build. Mater.* **2021**, *268*, 121079. [CrossRef]
56. Water Molecule Vibrations with Raman Spectroscopy. PhysicsOpenLab. Available online: https://physicsopenlab.org/2022/01/08/water-molecule-vibrations-with-raman-spectroscopy/ (accessed on 19 October 2023).
57. Nehdi, M.L.; Suleiman, A.R.; Soliman, A.M. Investigation of concrete exposed to dual sulfate attack. *Cem. Concr. Res.* **2014**, *64*, 42–53. [CrossRef]
58. Toutanji, H.; Delatte, N.; Aggoun, S.; Duval, R.; Danson, A. Effect of supplementary cementitious materials on the compressive strength and durability of short-term cured concrete. *Cem. Concr. Res.* **2004**, *34*, 311–319. [CrossRef]